Two-dimensional electronic spectroscopy based on conventional optics and fast dual chopper data acquisition

Ismael A. Heisler[1,*], Roberta Moca[1], Franco V. A. Camargo[1,2] and Stephen R. Meech[1,*]

[1] *School of Chemistry, Norwich Research Park, University of East Anglia, Norwich NR4 7TJ, UK*

[2] *CAPES Foundation, Ministry of Education of Brazil, Brasília - DF 70040-020, Brazil;*

Abstract

We report a new experimental scheme for two-dimensional electronic spectroscopy (2D-ES) based solely on conventional optical components and fast data acquisition. This is accomplished by working with two choppers synchronized to a 10 kHz repetition rate amplified laser system. We demonstrate how scattering and pump-probe contributions can be removed during 2D measurements and how the pump probe and local oscillator (LO) spectra can be generated and saved simultaneously with each population time measurement. As an example the 2D ES spectra for cresyl violet were obtained. The resulting 2D spectra show a significant oscillating signal during population evolution time which can be assigned to an intramolecular vibrational mode.

*To whom correspondence should be addressed. E-mail: i.heisler@uea.ac.uk; s.meech@uea.ac.uk

I. Introduction

Since its first demonstration in the IR and visible spectral regions, two-dimensional (2D) spectroscopy has been developing both experimentally and theoretically pushing its capabilities further into the visible region and more recently into the UV.[1-4] The extra information accessible by measuring 2D spectra when compared to the traditional 1D nonlinear techniques, such as pump-probe spectroscopy, have become apparent in the last couple of years.[5] One example of an important process probed by 2D spectroscopy is energy transfer dynamics.[6-9] Indications of the presence of energy transfer can be gathered with 1D measurements, however it appears in a very intuitive way in 2D spectra and more importantly un-entangled with other processes.[10] Coupling between electronic states and energy transfer are closely related and when there are couplings between transitions they appear quite distinctly in 2D spectra.[11] Further, by controlling the polarization of the laser beams used to measure 2D spectra incisive information about the electronic and vibrational structure of coupled molecules and aggregates are obtained.[12, 13] Another example is the observation and characterisation of coherent phenomena which are manifested in many ways in 2D spectra.[14] For instance, by following the amplitude of a 2D map in a specific spectral region, it is possible to see oscillations which can be due to vibrational coherence or, in the case of coupled molecular systems, excitonic evolution.[15] This is one the main results from early 2D electronic spectroscopy performed on photosynthetic light harvesting systems, a result that has been hotly debated in literature.[16, 17] The problem has been to prove the source of this coherence which, as has been shown recently, might not be purely electronic in origin but could have a vibrational contribution as well.[17] Finally, the problem which plagues 1D spectroscopies is that it is impossible to distinguish the mechanisms producing line broadening of a given transition. 2D spectroscopy solves this problem because it is a form of photon echo spectroscopy which removes the inhomogeneous broadening contribution of a given line shape. Many results have now been obtained in the IR and visible spectral regions which feed into theoretical calculations and are enhancing our understanding of line shape broadening mechanisms.[18-20]

The main experimental difficulty in implementing 2D spectroscopy in the optical region of the electromagnetic spectrum is the maintenance of phase stability.[21] This problem is aggravated in the visible to UV spectral regions due to the short cycle duration time (for example 1.67 fs at 500 nm).[3] Part of this problem was solved recently by working on the full optical rotating frame during the coherence period.[22] This was achieved by an alignment using four noncolinear beams located on the corners of a square and where always pairs of pulses are moved by a delay stage instead of moving pulses independently. Another critical issue for 2D spectroscopy (indeed for any optical spectroscopic method) is to avoid or remove scattering contributions. Scattering of light into the same direction as the signal deteriorates the signal/noise and can create "ghost" peaks in 2D maps.[23]

Different experimental implementations have been proposed to tackle the phase stability and scattering problems.[24-28] All implementations have their advantages and disadvantages with no scheme, at least so far, having an overwhelming number of superior features. Intrinsically phase stable setups based on the pump-probe geometry were used initially in the IR region but now are also available in the visible and UV regions.[3, 27] In these schemes a pulse shaper is usually used to generate phase stable collinear pump pulses, with a known and adjustable relative phase. The probe beam can be either an attenuated replica of the pump or a spectrally broader white light continuum.[29] The advantage of this scheme is that the signal is generated collinearly with the probe beam so that it is heterodyned with the probe itself and therefore automatically phased. This means that the absorptive component will be generated with no further need to phase the signal according to the projection slice theorem. Some disadvantages include: a strong background contribution, lowering its sensitivity; no easy independent manipulation of beam polarization; contributions of collinearly propagating nonlinear signals; the lack of access to rephasing and non-rephasing signals separately in a straight forward manner. Recently new ideas were proposed to overcome many of these negative features.[23, 27]

Regarding the light scattering problem, a method first implemented by Brixner et al. has been widely used to remove scattering contributions.[24] In this scheme, usually used in non-collinear 2D

setups, shutters block and unblock sequentially different beams in order to measure different scattering contributions. The recorded terms are later subtracted from the main measurement. The main problem with this scheme is that it is a relatively slow measurement method and does not allow shot-to-shot acquisitions. On the other hand a method recently developed by Zigmantas et al uses two choppers phase locked to the laser repetition frequency.[28] Each chopper modulates one beam with a given frequency. The signal is detected through a lock-in amplifier at the sum or difference frequencies of the modulation introduced by the choppers. This scheme is able to remove quite efficiently the scattering contributions and measurements can be done rapidly, roughly determined by the chopper frequencies. However, because lock-in acquisition implies some integration, it is not possible to perform shot-to-shot acquisitions. Finally, for 2D schemes based on the pump-probe geometry, scattering is usually removed through a phase cycling scheme.[27]

In this work we propose a hybrid scheme which relies on the best features of earlier proposed experimental implementations. It is based on the boxcar geometry using two beamsplitters to generate the four phase coherent beams.[22] Working with a 10 kHz repetition laser system, we used two choppers. With a fast acquisition CCD camera, we are able to measure every laser shot and perform the required subtractions of scattering contributions in real time. Also, by ordering the different acquired terms, for every population time the LO and pump-probe spectra are automatically generated and saved, accelerating the measurement process significantly. As test system we measured the 2D spectra of cresyl violet, a well know organic dye molecule which presents coherence dynamics during the population time.[15]

II. Principles of 2D spectroscopy

The fundamental theory of 2D spectroscopy has been presented in detail before.[30] Therefore discussion here will be restricted to its basic formalism without the details laid out explicitly in existing literature.[9] 2D electronic spectroscopy is a third-order nonlinear optical method entailing two time delays, three electromagnetic field interactions and signal generation. In a simplified form the electric field can be written as: $\mathrm{E}(t) = \mathrm{A}(t)e^{-i\omega t + i\mathrm{k.r}+\varphi} + \mathrm{c.c.}$, where $\mathrm{c.c.}$ stands for the

complex conjugate. The important features to highlight are: $\mathrm{A}(t)$ is the pulse envelope which for the experiments carried out in this work was a Gaussian with typical duration around 15 fs; ω is the pulse carrier frequency; k is the wave vector which determines the direction of beam propagation; φ is the phase which should be sufficiently stable to allow signal measurement with interferometric precision. For three electromagnetic fields interacting with a molecular system we have control over two relative delay times. A schematic of the pulse sequence with the definition of the relative delay times is shown as an inset in Figure 1a. Time is running from left to right meaning that the pulse on the left arrives earliest. For resonant laser pulses the molecular system can be thought of as being described by two electronic states, for example, ground state and first excited state (though more complex multi-state systems with vibronic levels can be incorporated). Under equilibrium conditions the vast majority of molecules will be in the ground electronic state. The effect of the first pulse is to create a superposition of the two states, a coherence, which is not a quantum mechanical stationary condition and therefore will evolve with a frequency ω_{eg}, proportional to the energy difference between ground (g) and excited (e) states. Hence, the interval between pulses 1 and 2, τ, is usually called the coherence time. The second pulse converts the superposition into a population state - either the ground or excited state - and thus the interval between pulses 2 and 3, *T*, is called the population time.[24] Finally, the third pulse converts the population into a superposition of quantum states producing a macroscopic oscillating polarization. This nonlinear polarization is the source of an electric field, $\mathrm{E}_{sig}(t) \propto i\,\mathrm{P}^{(3)}(t)$, which appears during emission time t. The nonlinear polarization, $\mathrm{P}^{(3)}(t)$, contains all of the information about the material interaction with the incoming electric fields. The third order nonlinear polarization is calculated through perturbation theory and can be written as:[9, 24]

$$\mathrm{P}^{(3)}(t) = \int_0^\infty dt_3 \int_0^\infty dt_2 \int_0^\infty dt_1\, \mathrm{R}^{(3)}(t_1, t_2, t_3)\,.\,\mathrm{E}(t-t_3)\mathrm{E}(t-t_3-t_2)\mathrm{E}(t-t_3-t_2-t_1). \qquad (1)$$

In the experiment, the laser beams propagate non-collinearly (Figure 1b) and therefore the signal electric field will be emitted into a well-defined spatial direction given by the wave vector phase-

matching condition: $\mathrm{k_s} = \pm\mathrm{k_1} \pm \mathrm{k_2} \pm \mathrm{k_3}$. The response function tensor, $\mathrm{R}^{(3)}(t_1, t_2, t_3)$, describes the material properties and is given by the sum over various contributions which can be laid out in terms of Feynman diagrams.[30]

In the heterodyne detection scheme a fourth electric field, usually called the local oscillator, is made to propagate along the same direction as the signal electric field and therefore interferes with it (Figure 1b). The measured signal is written as $S^{(3)}(t, T, \tau) = \mathrm{E}_{sig}(t, T, \tau)\mathrm{E}^{*}_{LO}(t)e^{-i\varphi_{LO}}$, where the coherence time, τ, and population time, T, have been written explicitly. Importantly, the final phase of the signal is given by the phase contribution from each incoming laser pulse plus the relative local oscillator phase, φ_{LO}. Typically the signal is measured along the phase matching direction given by $\mathrm{k_s} = -\mathrm{k_1} + \mathrm{k_2} + \mathrm{k_3}$, therefore the phase acquired by the signal is $\varphi_s = -\varphi_1 + \varphi_2 + \varphi_3 - \varphi_{LO}$.

A 2D measurement consists in the acquisition of the signal $S^{(3)}(t, T, \tau)$ for a series of population times T. For each population time the relative delay times τ and t need to be scanned with sub cycle precision. The data, however, is not usually presented in the time domain but rather in the frequency domain, requiring a double Fourier transformation over τ and t leading to $S^{(3)}(\omega_t, T, \omega_\tau)$. Since we use spectral interferometry[31] to measure the signal field, which implies using a spectrometer to measure the signal in the spectral domain, only a single Fourier transform along τ is needed to generate the final 2D frequency map. This complex signal carries absorptive and dispersive information.[9] Therefore it is critical to know precisely the phase between real and imaginary parts. The correct phase is retrieved by applying the projection-slice theorem[32] where the integral of a given 2D map over ω_τ is compared to the pump-probe measurement for the same population time. The phase is then adjusted until those two quantities match.

III. Experimental setup

A. Femtosecond laser system

The light source for the experiment is composed of a commercial amplified laser system plus a commercial non-collinear parametric amplifier (NOPA). The amplifier was a regenerative Ti:Sa

system (Spectra Physics Spitfire ACE pumped by an Evolution laser and seeded by MAITAI oscillator) delivering 500 μJ pulses at a central wavelength of 800nm and with a temporal duration of 120 fs and repetition rate of 10 kHz. Around 90% of the power was used to pump the NOPA system (TOPAS White, Light Conversion). The central wavelength delivered by the NOPA could be tuned in the region from 490 nm to 750 nm with typical pulse durations around 15 fs. Even though the NOPA system has an internal prism compressor which can be used to compensate chirp induced by external material it was necessary to direct the beam through a further external prism compressor. The typical NOPA output power at 550 nm was around 400 mW which at 10 kHz yields 40 μJ per pulse. Therefore after the external prism compressor a neutral density filter was used to reduce the power to around 4 mW in order to perform the experiments. The stability of the NOPA output given by the pulse to pulse fluctuation was typically below 0.5% rms for the central wavelength of the pulse spectrum.

B. Two-dimensional spectrometer setup

The experimental setup is based on an earlier development using only conventional optics.[22] The main difference in this setup compared to other 2D IR and 2D visible schemes is that it uses two beamsplitters to generate the four phase coherent beams and two mechanical delay stages which move synchronously to introduce the coherence delay time and the population time. Figure 1 shows a scheme of the setup. The critical issue in performing 2D spectroscopy is to maintain the laser pulse phase stability throughout a measurement. Many things can contribute to the generation of small vibrations of the optical elements in the setup, and therefore create small fluctuations of the path lengths of the beams, which correspond to phase fluctuations. One way of partially avoiding this is to move pulses in a pairwise manner so that path length fluctuations become anti-correlated and compensate each other.[33]

The input beam power was about 4 mW. The beam is steered into the setup with two mirrors and its alignment is checked with two irises on the entrance to the setup. Further irises inside the setup aid the daily alignment reproducibility. The first beamsplitter, BS1, creates two phase coherent

beams at different heights. The beamsplitters were tailor made through thin film deposition on 500 μm thick fused silica windows (Vortex Optical Coatings). The average transmission/reflection is approximately 50% for the spectral region between 350nm and 950nm. The separation of the beams is around 2.5 cm and the lowest beam is 7 cm away from the plane of the optical table (beams are kept as close as possible to the table to avoid large angular oscillations in the optical mounts which could introduce phase errors). The upper beam will later be split in to beams 3 and 4 and the lower into beams 1 and 2. The upper beam is steered towards a pair of delay stages which are mounted one on top of the other. The lower delay stage (Newport, UTS100CC), DS1, is able to move over a 100 mm distance (~600 ps) with a bidirectional precision of 2 fs. The upper delay stage, which is a piezo mover (Physik Instrumente, P-622.ZCD), PZ1, can travel over a 250 μm range (~1.5 ps) with a precision around 50 as. The initial alignment is such that the distance travelled by the upper beam is equal to the lower beam, that is, the delay stage compensates the extra 2.5 cm travelled by the lower beam. The upper and lower beams are then divided a second time by two beamsplitters, BS2, so that in total there are four phase coherent beams spatially located on the four corners of a square with equal distances between them of 2.5 cm (Figure 1b). Beams 1 and 3 are steered towards a second delay stage, PZ2, which is a similar piezo mover to PZ1. The initial alignment of this delay stage is such that it compensates the extra distance travelled by beams 2 and 4 after beamsplitters BS2. Finally the four beams hit a spherical mirror, SM, with a focal length of f = 15 cm, which focuses them to a common spatial position. The beams are then steered sideways with folding mirror, FM.

There are two choppers in the setup, C1, which modulates beam 2 and C2, which modulates beam 3. The chopper operation will be discussed in more detail in a subsequent section but, in summary, through their action on beams 2 and 3 it is possible to remove (from the total intensity measured by the detector) the contributions from the LO beam spectrum (chosen to be beam 4), from the pump-probe spectrum, and light scattering contributions which are emitted along the same direction as the LO beam. The sample is positioned where the four beams overlap. After the sample beams 1 to 3 are blocked and the LO is collimated and steered into a homemade polychromator.[34]

The polychromator consists of a highly dispersive prism (flint glass) which spatially disperses the wavelengths composing the broad spectrum of the LO beam. The spatially dispersed spectrum is imaged with a 20 cm focal length lens onto a CCD camera. Finally, the camera acquires independently each laser shot emitted by the laser. Additionally, each beam passes through an achromatic half wave plate, W, so that the polarization of each beam can be adjusted independently. The LO beam is attenuated by a variable neutral density filter, ND, and is delayed around 400 fs relative to the other beams by travelling through a fused silica plate.

C. Detection system

The spectrally dispersed LO beam is measured by a multichannel CCD camera. The camera used in the experiment consisted of a line scan camera with 1x1024 pixels (e2v AVIIVA EM1). The line acquisition rate can be adjusted up to 77 kHz and is therefore more than adequate to acquire each laser shot at 10 kHz. The camera is triggered at 10 kHz by the laser TTL signal and in its turn is able to send a TTL signal to a voltage acquisition board, allowing the acquisition of the TTL signal output of the two choppers. Therefore for each camera acquisition the state of each chopper is also acquired which enables the software to determine if beams 2 and 3 were (un)blocked when the LO pulse was acquired by the CCD camera. Ideally chopper C1 should operate at 5 kHz therefore blocking every other laser shot. However the high rotating speed required to operate at 5 kHz, would generate turbulence and air currents inside the 2D spectrometer, so the frequency of this chopper is set to 1kHz. Therefore 5 laser shots are blocked and the next 5 shots are transmitted (see Figure 2). Due to the beam size and the chopper slot size the border shots need to be discarded because they may be partly blocked. Therefore once the camera is triggered to start acquisition, a delay is added so that the first shot is ignored. The camera integration time is set to 300 μs therefore it integrates 3 shots and ignores the final 5^{th} shot. The signal is obtained by subtracting the acquisition with beam 2 present from the acquisition when beam 2 is blocked. A second subtraction of pairs of acquisitions for the situation when beam 3 is present or absent enables the removal of

unwanted contributions like pump-probe signals and scattering contributions from beams 1, 2 and 3, as described next.

D. Pump-Probe Measurement and Scattered Light Removal

One of the major problems affecting the signal/noise in 2D measurements is the contribution of unwanted light scattered in the same direction as the LO and signal beams. The scattered light comes mainly from beams 1, 2 and 3 and is phase coherent with the signal and LO beams and therefore also generates interferometric signals.[24] Apart from that, the LO beam itself can be contaminated with pump-probe signals. This can happen when the LO pulse arrives later than any of the three other beams and therefore acts as a probe beam for the transient absorption induced on the sample by any of the beams 1, 2 or 3. Different procedures to remove those unwanted contributions were proposed in literature, including the use of shutters and double modulation together with lock-in detection.[24, 28] The use of shutters significantly slows down the acquisition of the signal and does not allow shot to shot subtraction. In the case of double modulation of beams with lock-in detection it is desirable to work with lasers with high repetition rates. The scheme used in this work is intermediate given that the choppers also act like shutters, the advantage being that they are synchronized to the laser repetition rate which in principle allows shot-by-shot measurements even up to 5 kHz. In order to remove unwanted contributions from the signal we developed a scheme where choppers block and unblock beams 2 (k_2) and 3 (k_3). Figure 2 shows a schematic for the effect of the choppers on the beams. The laser repetition rate is 10 kHz and C1 is synchronized to 1/10 of this frequency, that is, its frequency is 1 kHz. In this case as Figure 2 illustrates, 5 laser shots are blocked and 5 shots are transmitted; the letters *a*, *b*, *c* and *d* label the 4 different chopper conditions for the two beams. The CCD camera acquisition by its turn is synchronized to the laser frequency and therefore acquires synchronously 5 LO laser shots when beam 2 is blocked (b/d) and 5 LO laser shots when beam 2 is unblocked (a/c). C2 is synchronized to half the frequency of C1, therefore its cycle completes every 2 ms. This means that for every pair of

blocked/unblocked events of beam 2, beam 3 will be blocked (c+d) and unblocked once (a+b) . A tailor made software routine subtracts the different cases from each other in the following order:

$$\alpha = a\text{-}b = |S_1 + S_2 + E_{LO}|^2 - |S_1 + E_{LO}|^2 = |S_2|^2 + 2Re\{S_1 S_2^*\} + 2Re\{S_2 E_{LO}^*\} \quad (2)$$

$$\beta = c\text{-}d = |S_1 + S_2 + S_3 + E_S + E_{LO}|^2 - |S_1 + S_3 + E_{LO}|^2 =$$

$$= |E_S|^2 + |S_2|^2 + 2Re\{S_1 S_2^*\} + 2Re\{S_2 E_{LO}^*\} + 2Re\{S_1 E_S^*\} + 2Re\{S_2 E_S^*\} + 2Re\{S_3 E_S^*\} + 2Re\{S_2 S_3^*\} + 2Re\{E_S E_{LO}^*\} \quad (3)$$

$$\beta - \alpha = |E_S|^2 + 2Re\{S_1 E_S^*\} + 2Re\{S_2 E_S^*\} + 2Re\{S_3 E_S^*\} + 2Re\{S_2 S_3^*\} + 2Re\{E_S E_{LO}^*\} \quad (4)$$

In these equations, S_n, stands for the contributions of pump-probe signals originating from the interaction of LO beam and beams 1, 2 and 3 as well as scattering contributions from those beams into the direction of LO. For example, $S_1 = E_{s1} + \delta E_1$, has two contributions: the first, E_{s1}, is the pump-probe signal emitted along k_{LO} for the case where $E_1 = \sqrt{I_1(\omega)}e^{i\varphi_1(\omega)+i\omega t_1}$ acted as a pump and E_{LO} acted as a probe; the second term δE_1 corresponds to a small fraction of Rayleigh light scattering of beam E_1 into the direction k_{LO} quantified by a constant δ. The first five contributions in equation (4) are phase coherent with the LO and therefore will interfere on the detector. However their interferograms will have different modulation frequencies given that the time delay relative to LO depends on the positions of delay stages DS1 and PZ2.[24] The term E_S stands for the electric field originating from the diffraction of beam 3 from the transient grating formed by beams 1 and 2. This signal is the only relevant contribution to the 2D measurement. Therefore only term $2Re\{E_S E_{LO}^*\}$, given by the transient grating signal heterodyned by the local oscillator field, in equation (4) should be isolated for posterior Fourier transformation. Even though it seems that there are still many scattering terms present it is important to notice that the main scattering contributions given by interferences with E_{LO} have been removed. The remaining contributions are all centred on different (relative to LO pulse) delay times and are weak. For example terms like $2Re\{S_n E_S^*\}$ originate from the interference of the signal field with scattering contributions and are therefore bound to make

small contributions. Further, those terms will be removed by Fourier windowing during the spectral interferometry procedure which is applied to equation (4).[24] The only terms to survive will be the ones which are centred around t_s - t_{LO}, that is the time delay between signal and LO pulses. It is important to reiterate that a key advantage of using a second chopper is that the term $2Re\{S_2 E_{LO}^*\}$ which appears in equation (3) has been removed. This term represents the pump-probe signal generated by the interaction of beams 2 and LO with the sample and can be significant for samples with strong transient absorption signals. Figure 3a shows an example of a 2D plot of a series of interferograms taken for different coherence times. For each coherence time, the measured interferogram is given by the end result *R*. Figure 3b shows a measured interferogram for coherence time τ = 0 fs.

Another major advantage of working with two choppers is that the pump-probe and the LO spectra for each population time can be measured together with the 2D signal measurement, under the same experimental conditions. In order to illustrate this procedure Figure 2 showed a cartoon for the action of the choppers on the 3 excitation beams. For case *b* above, where beams 2 and 3 are blocked, the LO spectrum can be measured independently as seenin Figure 2 (case *b*). Even though beam 1 is also present at the sample it is delayed relative to LO beam so that it cannot create any pump-probe contamination. In order to measure the pump-probe signal for a given population time, the term α, given by equation (2), is measured. This is the condition where beam 3 is blocked and illustrated by cases *a* and *b* in Figure 2. In this case, the LO pulse is moved back in time with DS1 by the same delay determined at the start of the experiment as being the LO delay (~ 400 fs), and is therefore overlapping temporally with beam 3. After this procedure DS1 returns to its original position determined by the population time delay and the coherence time is scanned producing the full 2D measurement (Figure 3). A typical measurement for 100 coherence time steps and an average of 1000 laser shots per delay time, including collection of the pump-probe signal and LO spectrum, is performed during a time of 3 minutes. Therefore in 1 hour around 20 2D spectra can be [illegible]

E. Delay Stages Movement Sequence

The proper sequence of delay stage movements in this experimental scheme is critical to obtaining correct 2D measurements. In order to illustrate the procedure, Figure 4 presents the cases of rephasing and non-rephasing signal measurements.[9] The rephasing signal is measured along the phase matched direction, $\mathrm{k_s} = -\mathrm{k_1} + \mathrm{k_2} + \mathrm{k_3}$,which contains a signal with approximate oscillatory factor $e^{i\omega(\tau - t)}$ and therefore, for a detection time equal to coherence time, $t = \tau$, a maximum in emission occurs, also called the photon echo.[24] The non-rephasing signal is emitted along the phase matched direction, $\mathrm{k_s} = -\mathrm{k_1} + \mathrm{k_2} + \mathrm{k_3}$, and does not produce an echo burst because the oscillatory term $e^{i\omega(\tau + t)}$ does not allow rephasing of the signal. Experimentally both signals can be measured along the same spatial direction by switching the order of arrival of pulses 1 and 2.[35]

Initially the LO pulse acquires a fixed delay relative to pulses 1, 2 and 3. Specifically for this experimental setup the LO pulse arrives ahead in time by around 400 fs. In Figure 4 the LO pulse is illustrated by the dashed Gaussian and appears at positive detection times. Population time zero is determined either when all the pulses are temporally overlapped or either pulse 1 or 2 is temporally overlapped with pulse 3. This is the time origin for the coherence and detection timescales. The timescale running from zero to the right, +*t*, corresponds to the detection timescale for both rephasing and non-rephasing cases. In Figure 4, the coherence timescale, τ, runs to the left of population time zero and is negative for the non-rephasing case and positive for the rephasing case. For the non-rephasing case pulse 2 moves increasingly to the left and therefore acquires larger negative coherence delay times. For the rephasing case pulse 1 moves increasingly to the left and therefore acquires larger positive coherence delay times. As already mentioned the population time is defined as being the time between the arrival (at the sample position) of the second pulse (either pulse 1 or 2) and pulse 3. When performing an experiment, initially the population time is set to some relevant value, by DS1. As illustrated in Figure 4, by changing relative delays of pulses 1 (by moving delay stage PZ2), the LO pulse will also move relative to pulse 3. However that does not modify the relative delay between LO and signal emission maximum. This is more clearly illustrated

for the rephasing case where there is an echo emission, as illustrated in Figure 4. Even though for the non-rephasing case this concept is not so easy to visualize the same principle applies. In order to generate negative coherence times pulse 2 has to arrive earlier than pulse 1 on the sample. Therefore, delay stage PZ2 has to be moved forwards, which means that pulses 1 and 3 move relative to pulse 2. In this case time zero is shifted because it is defined by the arrival of pulse 3. For example if coherence time was incremented by a value of -$\Delta\tau$ the relative delay between pulse 3 and LO decreases by this same amount -$\Delta\tau$. As will be shown later, this translates into a phase change which exactly compensates the phase change being measured by changing the coherence time. For positive coherence times (rephasing case in Figure 4), pulse 1 has to be the one to arrive earlier then pulse 2 on the sample. Therefore initially PZ2 is moved backwards which means that pulses 1 and 3 arrive earlier than pulse 2. However this also means that the population time has been changed because the second pulse to arrive at the sample is now pulse 2. Therefore PZ1 has to be moved by the same amount +$\Delta\tau$ forwards to compensate for the population time. But when this happens LO pulse is also moved by the same amount +$\Delta\tau$.

The delay stage movements introduced in this manner lead to the natural measurement of the signal in the rotating frame.[23] This happens because of LO pulse movement relative to pulse 3, as shown next. The phase of the signal being measured can be written as $I_{sig}\sim e^{-i(\Delta\varphi_{1,2}-\Delta\varphi_{3,LO})}e^{-i\omega(\tau-t)} = e^{-i\Delta\varphi_{1,2}}e^{i(\Delta\varphi_{3,LO}-\omega\tau)}e^{i\omega t}$, where $\Delta\varphi_{1,2} = \varphi_1 - \varphi_2$ and $\Delta\varphi_{3,LO} = \varphi_3 - \varphi_{LO}$. We can also define the LO relative phase as $\Delta\varphi_{3,LO} = \omega t_{LO}$. From the previous discussion we know that if the coherence time is changed by positive amounts, $\tau'=\tau+\Delta\tau$, then the local oscillator moves oppositely, that is, $t'_{LO} = t_{LO}-\Delta\tau$, therefore from the above equation one can immediately see that the phase difference being measured by changing the coherence time is offset by the phase alteration introduced by the LO pulse movement. Thus, when a delay stage moves to change the relative coherence time it will also move the local oscillator (LO) pulse creating a net phase change which is zero. One advantage of this scheme is that the phase stability only has to be maintained to within a fraction of the duration of the laser pulse (typically around 15 to 20 fs)

compared to a fraction of the period of a single oscillation (1.67fs for 500 nm). However the phase stability during the detection time still depends critically on relative movements of the LO pulse against the signal requiring stable optical mounts and no strong air currents in the setup. The phase stability condition of the setup as discussed next.

F. Phase Stability

The total phase acquired by the signal electric field is determined by choosing a given spatial direction along which the phase matched signal field is emitted. For the rephasing phase matched direction (Figure 1b), $k_s = -k_1 + k_2 + k_3$, the total phase of the heterodyne detected 2D ES signal is given by:

$$\Delta\varphi_s = -\varphi_1 + \varphi_2 + \varphi_3 - \varphi_{LO} + \varphi_{sig} = (\varphi_2 - \varphi_1) + (\varphi_3 - \varphi_{LO}) + \varphi_{sig} \quad (5)$$

where φ_{sig} is the phase produced by interaction of the laser electric fields with the sample.[36] Therefore, phase fluctuations in each beam produce an overall phase fluctuation as follows:

$$\delta(\Delta\varphi_s) = (\delta\varphi_2 - \delta\varphi_1) + (\delta\varphi_3 - \delta\varphi_{LO}) \quad (6)$$

It is possible to trace the contributions to the phase fluctuations contributing to each term of the equation above by acknowledging the contribution of each optical element in the setup (Figure 1a).[36] For example, the equation below shows explicitly the contributions for one of the phase terms (other terms can be obtained by following the beam path (Figure 1) in the same manner):

$$\delta\varphi_1 = \delta\varphi_{BS1} + \delta\varphi_{M1} + \delta\varphi_{BS2L} + \delta\varphi_{PZ2+P2} + \delta\varphi_{SM} + \delta\varphi_{FM} \quad (7)$$

Taking the respective differences of the above terms results in

$$\delta\varphi_2 - \delta\varphi_1 = \delta\varphi_{M2} - \delta\varphi_{PZ2+P2} \quad (8)$$

$$\delta\varphi_3 - \delta\varphi_{LO} = \delta\varphi_{PZ2+P2} - \delta\varphi_{M2} \quad (9)$$

Therefore, due to the anti-correlation of the fluctuations, adding equations (8) and (9) results in phase fluctuations equal to zero. In this analysis, single beam fluctuations are not considered but

these can become significant, for example if there are air currents which affect differently the individual beam paths. However, even though the phase difference of the different beam pairs fluctuates significantly during even short periods of time due to their anti-correlation, those fluctuations cancel out almost perfectly and therefore the overall phase of the measured signal is much more stable.[33] To ensure the overall phase stability of the setup the optical components are assembled in a compact manner on the bench (total footprint of 30cm x 50 cm), and the setup is enclosed in a box to minimize any air currents.

IV. Experimental Results

In order to demonstrate the capabilities of the high repetition rate dual chopper experimental setup we carried out measurements on the dye molecule cresyl violet (CV) perchlorate ($C_{16}H_{11}N_{3O}{\cdot}HClO_4$, MW=361.74), previously studied by Turner et al.[15] Such organic dye molecules typically have significant extinction coefficients in the visible spectral region with broad absorption bands often modulated by a progression of vibronic modes. The sample was purchased from Sigma Aldrich and dissolved in methanol without further purification. At the peak of the absorption (~ 596 nm) the optical density was 0.35 in a 1 mm path length cuvette. For the 2D spectra measurements the coherence time was scanned from -150 fs to +150 fs with 4 fs delay steps and for population times ranging from 30 fs to 500 fs in 5 fs steps. The energy per pulse was around 2 nJ at the sample position.

The linear absorption spectrum and the molecular structure of CV are shown in Figure 5a. The small shoulder at around 618 nm is due to the first vibronic overtone (ν = 18 THz), assigned to an orthogonal aromatic stretching mode in the central ring.[37] For the 2D measurements even though the laser spectrum had a bandwidth of 40 nm (producing pulses with 16 fs duration) it was not sufficient to cover the entire absorption band. Therefore the amplitude of the measured 2D spectrum will be modulated by the laser profile, as shown in Figure 5b which presents a 2D spectrum for a population time T = 130 fs. This spectrum consists of the absolute magnitude of the total signal (rephasing plus non-rephasing). The graph on top of the 2D map shows the linear absorption line

shape together with the laser spectrum. The shape of the 2D spectrum is clearly modulated by the laser spectrum double peak structure. Along the diagonal (dashed grey line) the 2D spectrum closely resembles the linear absorption spectrum, only narrower due to the fact that the excitation spectrum is narrower than the full absorption line shape. The quality of the "phasing" required for the separation of absorptive and dispersive responses can be seen in Figure 5c which compares the pump-probe measurement with the projection of the 2D spectrum onto the detection frequency axis, ν_3, for a population time T = 130 fs. The fact that the pump-probe signal was measured quasi-simultaneously with the measurement of the 2D spectrum and under identical experimental conditions increases the reliability and consistency of the comparison between pump-probe and 2D projection.

The 2D spectra have an almost rectangular shape. This hints at the presence of cross peaks connecting high frequency excitation with low frequency detection (and vice-versa). At lower frequencies the main contribution to the signal arises from the bleaching of the S_0 to S_1 electronic transition, centred at 596 nm, whereas at higher energies the vibronic shoulder contributes to the signal. This is corroborated by following the amplitude of different frequency positions along the 2D spectra. The selected four positions are indicated on the 2D map, Figure 5b. As shown in Figure 6a, the amplitude oscillates with a well-defined frequency for all four points. Additionally peaks 2 and 4 show a slow exponential relaxation whereas peaks 1 and 3 show an exponential growth on the same timescale followed by a slow relaxation. The black lines in Figure 6a on top of curves 3 and 4 were obtained by fitting these curves with a sum of exponential and damped cosine functions. For curve 3 an exponential growth could be fit with a time constant of 40 fs whereas curve 4 presents an initial relaxation with a similar 40fs timescale. This is a clear indication of energy transfer (relaxation) from higher to lower frequencies. Due to the intramolecular coupling this transfer can happen on a very fast timescale. The determination of this constant is probably limited by the time resolution of our instrument.

Finally by taking a Fourier transform of any of the oscillating peaks it was possible to recover a frequency centred at 586.5 cm^{-1} (17.58 THz), Figure 6c, which matches exactly the orthogonal stretching frequency present in CV determined previously by Raman spectroscopy. [37] The origin of these oscillations was explained as originating from nuclear wave packet dynamics. Similar oscillations can also be measured with transient absorption pump-probe measurements; however the advantage 2D spectroscopy is that the oscillating features can be assigned to specific excitation frequencies.

The results presented in Figures 5 and 6 demonstrate the ability of the 2D experimental setup described to obtain fast and reliable 2D spectra with good signal/noise. The advantages of the setup are: flexibility in terms of wavelength of operation (480nm up to 950nm) enabled by the use of conventional beamsplitters with broad reflective coatings; fast data acquisition with simultaneous collection of pump-probe and LO spectra; real time scattering and pump-probe contribution removal enabled by the use of two choppers.

V. Conclusion

In this paper we described a new 2D electronic spectroscopy setup based on conventional optics and fast data acquisition. Use of beamsplitters for the generation of the four phase coherent pulses enabled the setup to be used over the whole visible spectral region. This scheme can be thought of as a hybrid scheme which relies on the best features of earlier proposed experimental implementations. Working with a 10 kHz repetition laser system significantly accelerates the data collection. Importantly, by working with two choppers in conjunction with a fast acquisition CCD camera, we are able to measure every laser shot and perform the required subtractions of scattering contributions in real time. We also showed that by ordering different acquired terms, for every population time, the LO and pump-probe spectra are automatically generated and saved, accelerating the measurement process significantly. As a test system we measured the 2D spectra of CV. We were able to corroborate previously observed oscillations during the population evolution

time. The recovered frequency of this oscillation, 17.58 THz, was assigned to the orthogonal stretching vibrational mode of CV, previously determined by Raman spectroscopy. Also by fitting the dynamical evolution of the upper cross peak in the 2D spectra indicated energy transfer to lower frequencies on a timescale of 40 fs.

VI. Acknowledgements

This work was supported by EPSRC funding through grant EP/J009148/1 and J021431/1. We would like to thank Professor Tobias Brixner and Dr Patrick Nürnberger for advice on experimental setup and helpful discussions. Franco Valduga de Almeida Camargo is supported by Brazilian Funding Agency CAPES (Coordination for the Improvement of Higher Level Personnel) through a doctoral studentship (process number BEX 9527/13-3). Roberta Moca thanks UEA for the award of a studentship.

Figure Captions

Figure 1. (a) 2D ES experimental setup where: BS1,2 beamsplitters; P1,2 aluminium coated knife-edge right angle prisms; DS1 and PZ1,2 mechanical delay stages; C1,2 optical choppers; λ/2+FS half wave plates plus fused silica windows; ND neutral density filter; SM spherical mirror; FM folding mirror. The upper right corner illustrates the pulse arrival sequence on the sample as well as the signal emission and LO position in time relative to pulse 3. The left hand corner illustrates the home made polychromator composed of a mirror, highly dispersive prism, lens and CCD camera. (b) The beam geometry used in the setup.

Figure 2. Illustration showing the effects of the optical choppers on the different beams. Chopper C1 acts on beam 2 with a frequency of 1 kHz whereas chopper C2 acts on beam 3 with a frequency of 500 Hz. See text for description.

Figure 3. (a) Example of spectral interferograms measured with the 2D ES setup. (b) A slice from (a) showing a single spectral interferogram for a coherence time $\tau = 0$ fs.

Figure 4. Pulse arrival time ordering scheme for rephasing and non-rephasing cases. See text for description.

Figure 5. (a) Cresyl Violet Linear absorption spectrum. Inset shows molecular structure. (b) Representative absolute value 2D ES spectrum for cresyl violet at $T = 130$fs. The intensity is given by 21 evenly spaced contour lines (c) Comparison between the pump-probe signal and the projection onto the detection frequency axis of the 2D ES spectrum for a population time of $T = 130$fs.

Figure 6. (a) Intensity of single points marked on 2D spectrum (Figure 5a) as a function of population time. The black overlapping with curves 3 and 4 are the fit results as described in text. (b) Power spectrum obtained after Fourier transforming curve 2.

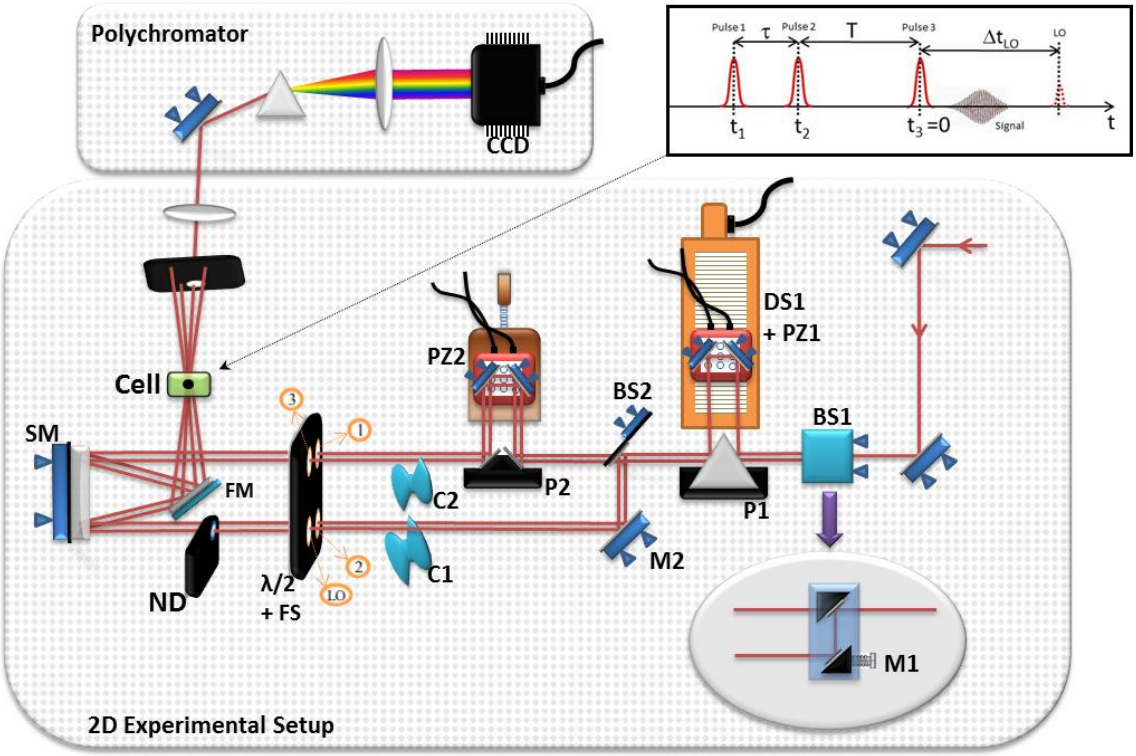

Figure 1a

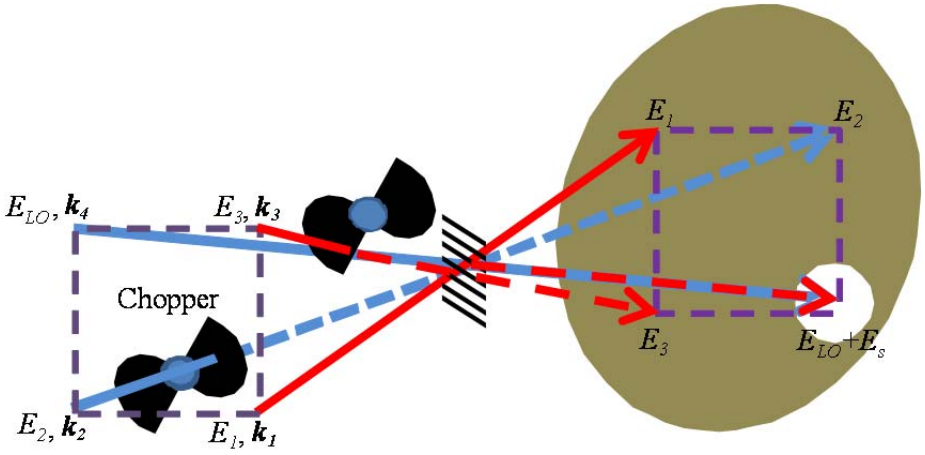

Figure 1b

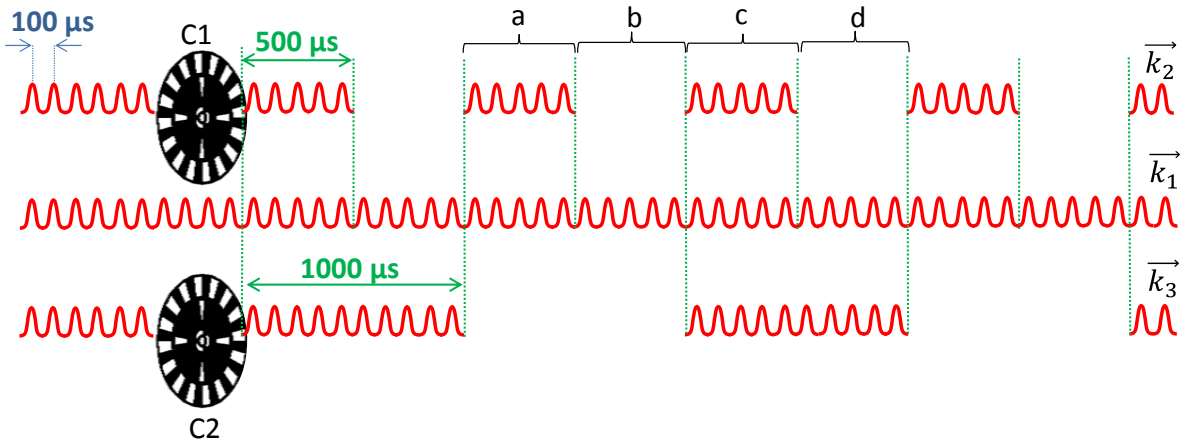
100 µs
C1
500 µs
a
b
c
d
$\overrightarrow{k_2}$
$\overrightarrow{k_1}$
1000 µs
$\overrightarrow{k_3}$
C2

Figure 2

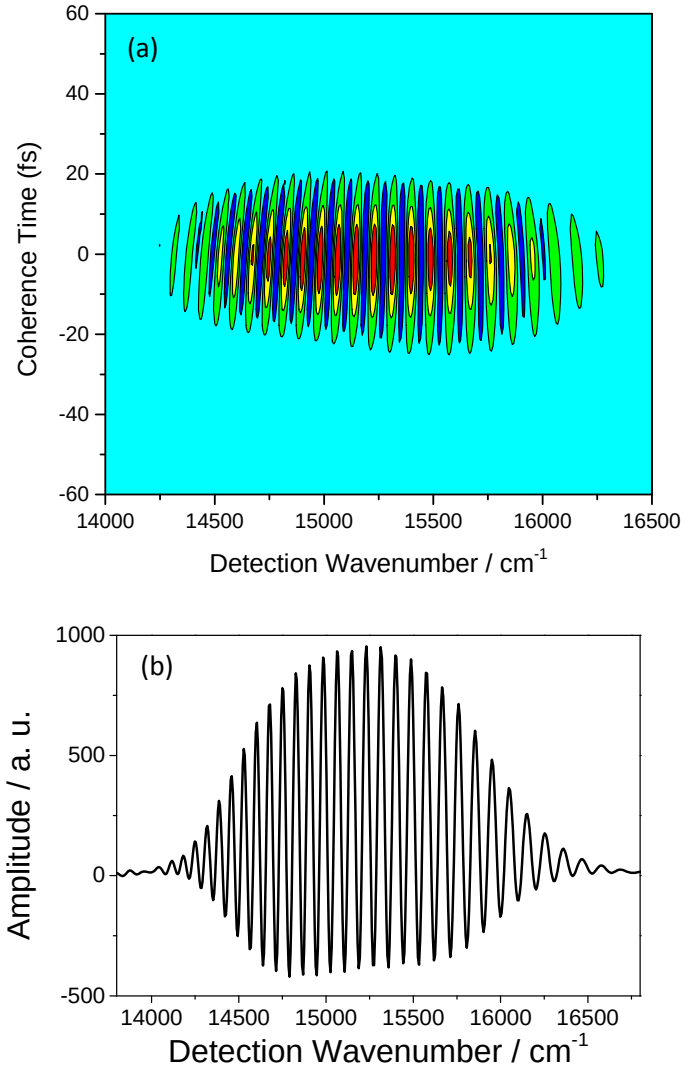
(a)
Coherence Time (fs)
60
40
20
0
-20
-40
-60
14000
14500
15000
15500
16000
16500
Detection Wavenumber / cm-1
(b)
Amplitude / a. u.
1000
500
0
-500
14000
14500
15000
15500
16000
16500
Detection Wavenumber / cm-1

Figure 3

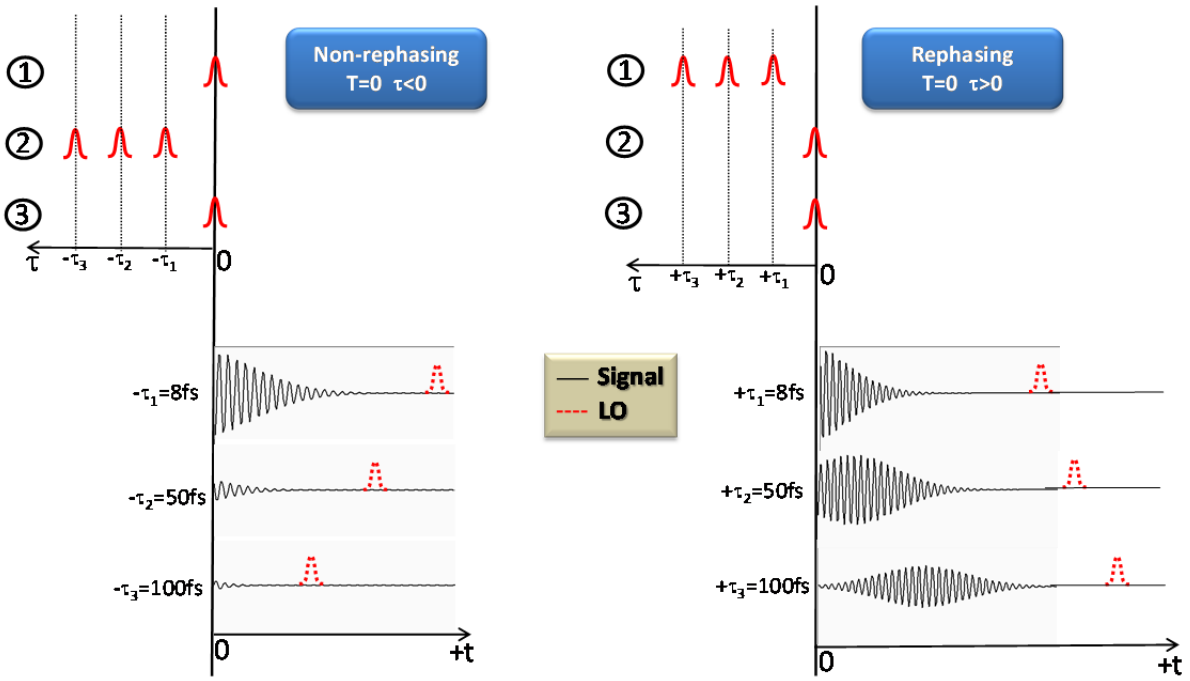
Non-rephasing
T=0 τ<0
Rephasing
T=0 τ>0
①
②
③
τ
-τ3 -τ2 -τ1
+τ3 +τ2 +τ1
0
Signal
LO
-τ1=8fs
-τ2=50fs
-τ3=100fs
+τ1=8fs
+τ2=50fs
+τ3=100fs
+t

Figure 4

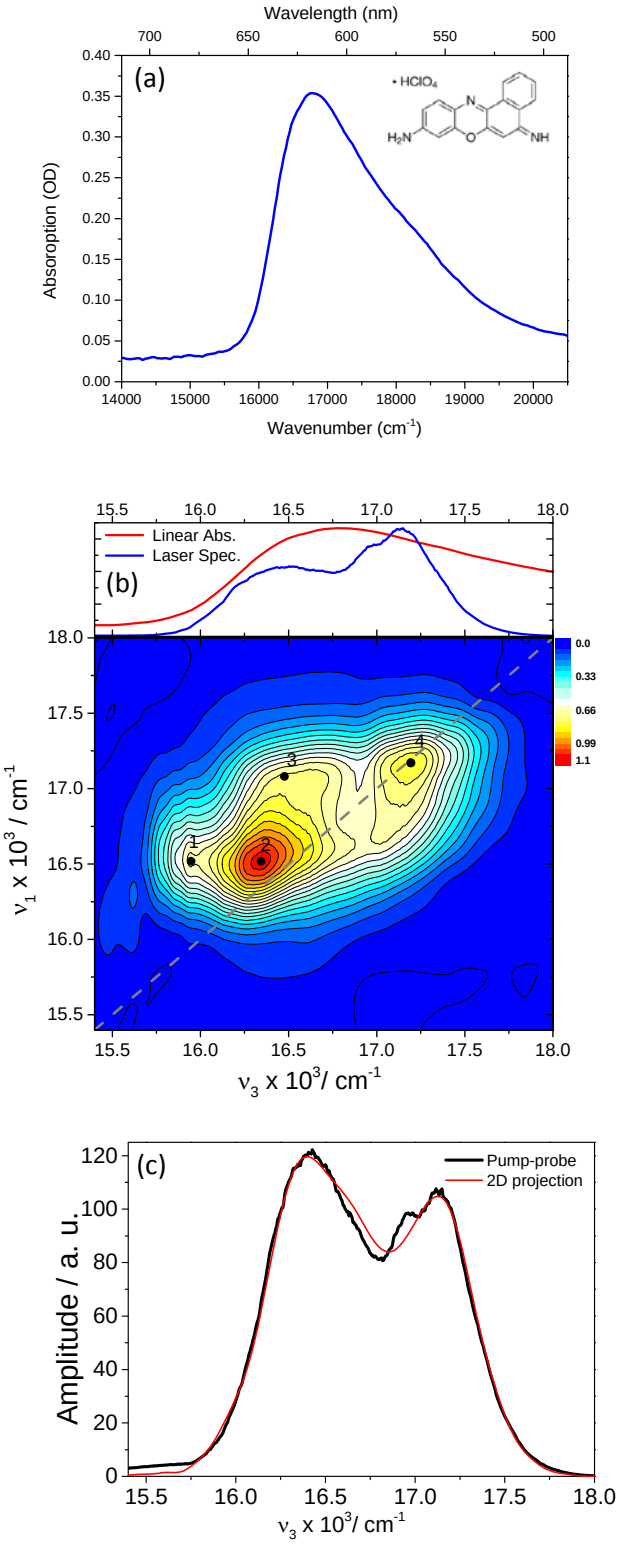
Wavelength (nm)
700
650
600
550
500
(a)
• HClO4
H2N
N
O
NH
Absoroption (OD)
Wavenumber (cm-1)
Linear Abs.
Laser Spec.
(b)
ν1 x 10^3 / cm-1
ν3 x 10^3/ cm-1
(c)
Pump-probe
2D projection
Amplitude / a. u.
ν3 x 10^3/ cm-1

Figure 5

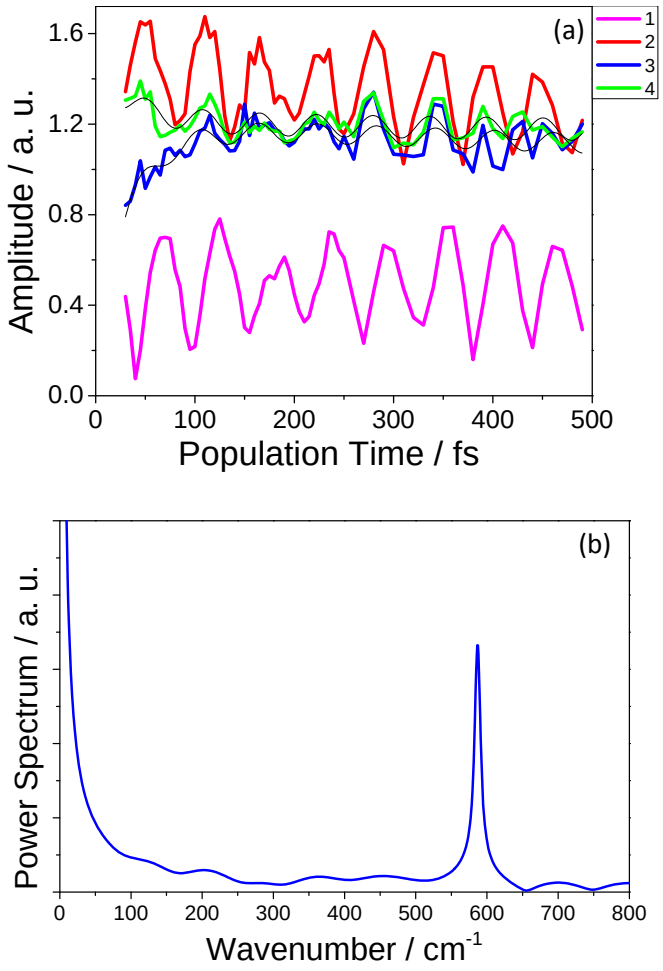
(a)
1
2
3
4
Amplitude / a. u.
1.6
1.2
0.8
0.4
0.0
0
100
200
300
400
500
Population Time / fs
(b)
Power Spectrum / a. u.
0
100
200
300
400
500
600
700
800
Wavenumber / cm-1

Figure 6

References

[1]P. Hamm, M. Lim and R. M. Hochstrasser, Phys. Rev. Lett. **81,** 5326-5329 (1998).
[2]J. D. Hybl, A. W. Albrecht, S. M. G. Faeder and D. M. Jonas, Chem. Phys. Lett. **297,** 307-313 (1998).
[3]N. Krebs, I. Pugliesi, J. Hauer and E. Riedle, New J Phys **15,** (2013).
[4]C. Consani, G. Aubock, F. van Mourik and M. Chergui, Science **339,** 1586-1589 (2013).
[5]E. E. Ostroumov, R. M. Mulvaney, J. M. Anna, R. J. Cogdell and G. D. Scholes, J. Phys. Chem. B **117,** 11349-11362 (2013).
[6]P. D. Dahlberg, A. F. Fidler, J. R. Caram, P. D. Long and G. S. Engel, Journal of Physical Chemistry Letters **4,** 3636-3640 (2013).
[7]A. F. Fidler, V. P. Singh, P. D. Long, P. D. Dahlberg and G. S. Engel, J. Chem. Phys. **139,** (2013).
[8]K. L. M. Lewis and J. P. Ogilvie, Journal of Physical Chemistry Letters **3,** 503-510 (2012).
[9]G. S. Schlau-Cohen, A. Ishizaki and G. R. Fleming, Chem. Phys. **386,** 1-22 (2011).
[10]T. Brixner, J. Stenger, H. M. Vaswani, M. Cho, R. E. Blankenship and G. R. Fleming, Nature **434,** 625-628 (2005).
[11]C. Greve, N. K. Preketes, H. Fidder, R. Costard, B. Koeppe, I. A. Heisler, S. Mukamel, F. Temps, E. T. J. Nibbering and T. Elsaesser, J. Phys. Chem. A **117,** 594-606 (2013).
[12]E. L. Read, G. S. Engel, T. R. Calhoun, T. Mancal, T. K. Ahn, R. E. Blankenship and G. R. Fleming, Proc. Natl. Acad. Sci. U. S. A. **104,** 14203-14208 (2007).
[13]J. E. Laaser and M. T. Zanni, J. Phys. Chem. A **117,** 5875-5890 (2013).
[14]N. Christensson, F. Milota, J. Hauer, J. Sperling, O. Bixner, A. Nemeth and H. F. Kauffmann, J. Phys. Chem. B **115,** 5383-5391 (2011).
[15]D. B. Turner, K. E. Wilk, P. M. G. Curmi and G. D. Scholes, Journal of Physical Chemistry Letters **2,** 1904-1911 (2011).
[16]G. S. Engel, T. R. Calhoun, E. L. Read, T. K. Ahn, T. Mancal, Y. C. Cheng, R. E. Blankenship and G. R. Fleming, Nature **446,** 782-786 (2007).
[17]A. Chenu, N. Christensson, H. F. Kauffmann and T. Mancal, Sci Rep-Uk **3,** (2013).
[18]R. Costard, I. A. Heisler and T. Elsaesser, The Journal of Chemistry Letters **5,** 506-511 (2014).
[19]C. J. Fecko, J. D. Eaves, J. J. Loparo, A. Tokmakoff and P. L. Geissler, Science **301,** 1698-1702 (2003).
[20]N. S. Ginsberg, Y. C. Cheng and G. R. Fleming, Accounts Chem. Res. **42,** 1352-1363 (2009).
[21]D. M. Jonas, Annu. Rev. Phys. Chem. **54,** 425-463 (2003).
[22]U. Selig, F. Langhojer, F. Dimler, T. Lohrig, C. Schwarz, B. Gieseking and T. Brixner, Opt. Lett. **33,** 2851-2853 (2008).
[23]P. Hamm and M. Zanni, *Concepts And Methods Of 2D Infrared Spectroscopy* (Cambridge University Press, Cambridge, 2011).
[24]T. Brixner, T. Mancal, I. V. Stiopkin and G. R. Fleming, J. Chem. Phys. **121,** 4221-4236 (2004).
[25]F. Milota, J. Sperling, A. Nemeth, T. Mancal and H. F. Kauffmann, Accounts Chem. Res. **42,** 1364-1374 (2009).
[26]T. H. Zhang, C. N. Borca, X. Q. Li and S. T. Cundiff, Optics Express **13,** 7432-7441 (2005).
[27]S. H. Shim and M. T. Zanni, Phys. Chem. Chem. Phys. **11,** 748-761 (2009).
[28]R. Augulis and D. Zigmantas, Optics Express **19,** 13126-13133 (2011).
[29]P. E. Tekavec, J. A. Myers, K. L. M. Lewis and J. P. Ogilvie, Opt. Lett. **34,** 1390-1392 (2009).
[30]M. Cho, *Two-Dimensional Optical Spectroscopy* (CRC Press, Boca Raton, 2009).
[31]C. Dorrer, N. Belabas, J. P. Likforman and L. Joffre, Applied Physics B-Lasers and Optics **70,** S99-S107 (2000).
[32]S. M. G. Faeder and D. M. Jonas, J. Phys. Chem. A **103,** 10489-10505 (1999).
[33]M. L. Cowan, J. P. Ogilvie and R. J. D. Miller, Chem. Phys. Lett. **386,** 184-189 (2004).
[34]U. Megerle, I. Pugliesi, C. Schriever, C. F. Sailer and E. Riedle, Applied Physics B-Lasers and Optics **96,** 215-231 (2009).

[35]M. Khalil, N. Demirdoven and A. Tokmakoff, J. Phys. Chem. A **107,** 5258-5279 (2003).
[36]V. I. Prokhorenko, A. Halpin and R. J. D. Miller, Optics Express **17,** 9764-9779 (2009).
[37]E. Vogel, A. Gbureck and W. Kiefer, J. Mol. Struct. **550,** 177-190 (2000).